Supplementary Information

Global survey of the immunomodulatory potential of common drugs

Gregory I. Vladimer[1‡], Berend Snijder[1,7‡], Nikolaus Krall[1], Johannes W. Bigenzahn[1], Kilian V.M. Huber[1,2], Charles-Hugues Lardeau[1,3], Kumar Sanjiv[4], Anna Ringler[1,3], Ulrika Warpman Berglund[4], Monika Sabler[1], Oscar Lopez de la Fuente[1], Paul Knöbl[5], Stefan Kubicek[1,3], Thomas Helleday[4], Ulrich Jäger[5], Giulio Superti-Furga[1,6*]

[1]CeMM Research Center for Molecular Medicine of the Austrian Academy of Sciences, 1090 Vienna, Austria
[2]Structural Genomics Consortium, University of Oxford, Oxford, UK and Target Discovery Institute, University of Oxford, Oxford, UK
[3]Christian Doppler Laboratory for Chemical Epigenetics and Anti-Infectives, CeMM Research Center for Molecular Medicine of the Austrian Academy of Sciences, 1090 Vienna, Austria
[4]Science for Life Laboratory, Division of Translational Medicine and Chemical Biology, Department of Medical Biochemistry and Biophysics, Karolinska Institutet, S-171 21 Stockholm, Sweden
[5]Department of Internal Medicine I, Division of Hematology and Hemostaseology, Medical University of Vienna, 1090 Vienna, Austria
[6]Center for Physiology and Pharmacology, Medical University of Vienna, 1090 Vienna, Austria
[7]Current affiliation: Department of Biology, Institute of Molecular Systems Biology, ETH Zurich, Zurich, Switzerland.

Correspondence to: gsuperti@cemm.oeaw.ac.at

Supplementary Results

Supplementary Figure 1

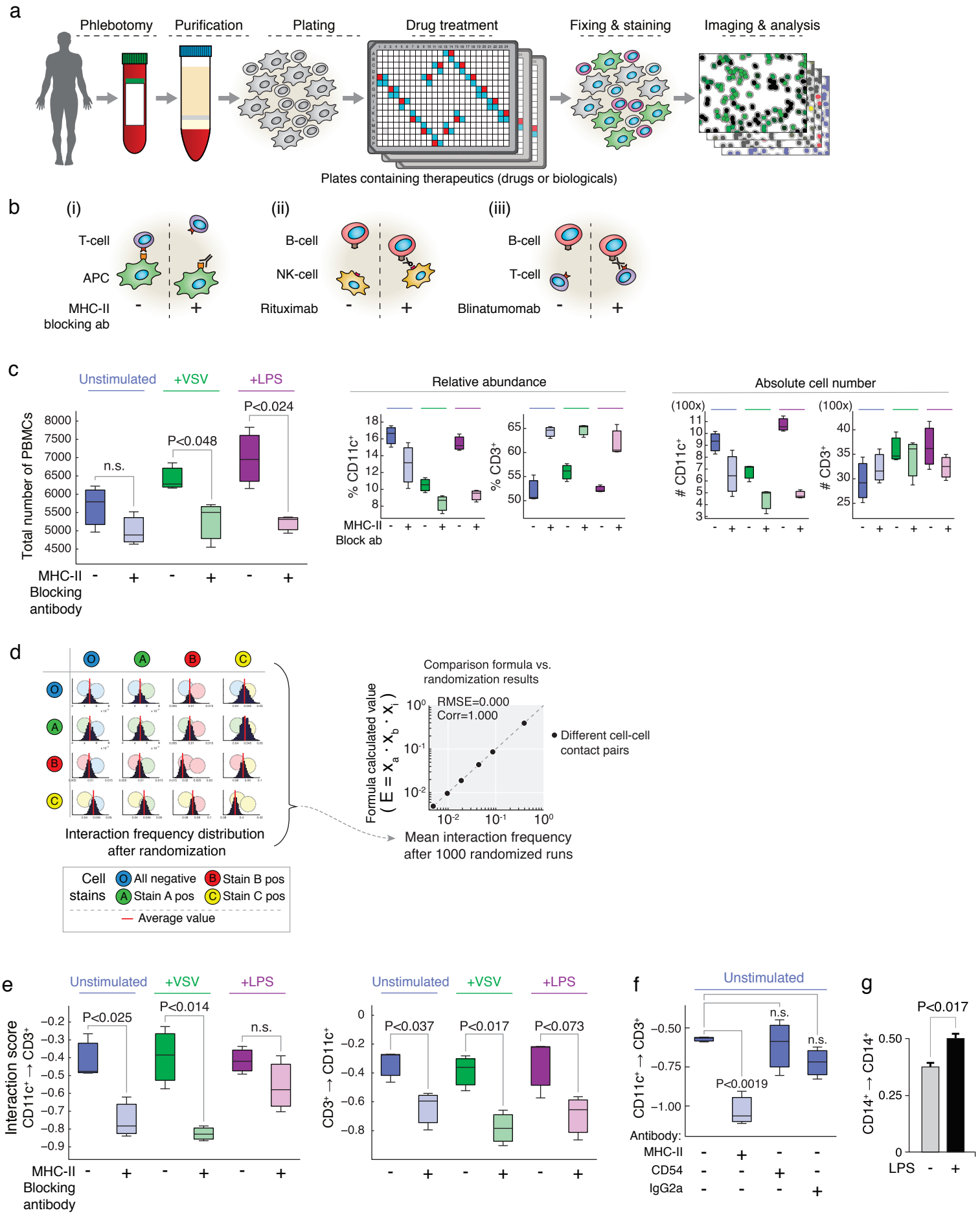

Supplementary Results

Supplementary Fig. 1. Image-based screening of PBMCs and the interaction score enables quantification of leukocyte cell-cell interactions, related to Figure 1

(a) Overview of screening pipeline used (images were 10x, 4-channel plus bright field). (b) Modes of action of biologicals used here: (i) anti-MHC-II blocking antibody, (ii) rituximab, and (iii) blinatumomab. (c) Analysis of healthy donor PBMCs with MHC-II directed antibody comparing (left) total number of PBMCs, (middle) relative abundance or (right) absolute number of $CD11C^+$ and $CD3^+$ cells. (d, left) Interaction frequency distributions between negative or three sets of single positive cell types after randomization; (d, right) mean interaction frequencies after 1000 bootstrap runs (x-axis) compared to the formula calculated value for the interaction score (y-axis). (e-g) Interaction score of (e) $CD3^+ \rightarrow CD11C^+$ cells after treatment with anti-MHC-II antibody and incubated with VSV, LPS, or naive, (f) $CD11C^+ \rightarrow CD3^+$ cells after incubation with anti-CD54 or IgG2a isotype control antibody, or (g) $CD14^+ \rightarrow CD14^+$ cells after stimulation with LPS. (c, e-g) Were performed in technical triplicates, average and boxplots or standard error of means over technical repeats are shown, and experiments are representative of two repeats from different healthy donors.

Supplementary Figure 2

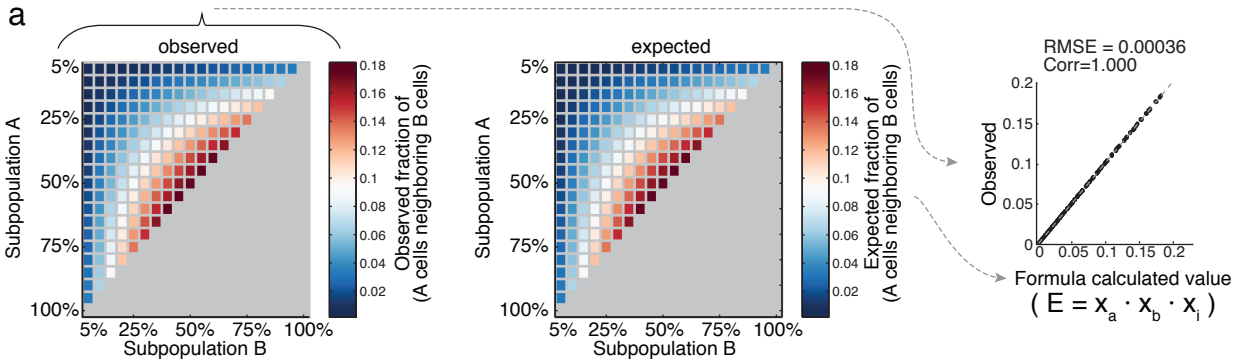

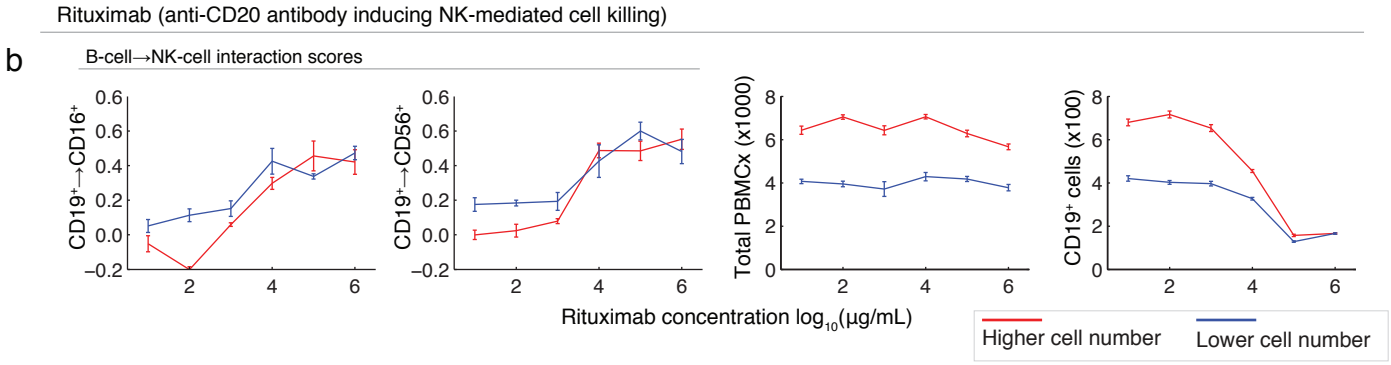

Supplementary Fig. 2. The interaction score is robust to changes in subpopulation cell number, relates to Figure 1

(a) Observed (left) or expected (middle) fraction of A cells → B cells after random assignment of cell identities to a fixed subpopulation (fixed positions of cells within one well with 15,140 cells) (right) the comparison of what is expected versus what is observed when using the interaction score to quantify A cell → B cell interactions with varying cell populations from panels left and middle. (b) Cell counts of (right) total PBMCs or (far right) $CD19^+$ cells, or interaction scores of (left) $CD19^+ \rightarrow CD56^+$ cells or (far left) $CD19^+ \rightarrow CD56^+$ cells after incubation with rituximab at increasing concentrations. Mean and standard error of means are shown for experiments at low (blue line) or higher (red line) total cell numbers. (b) Performed in 8 technical repeats, average and standard error of means over technical repeats are shown, and representative of at least two repeats from different healthy donors.

Supplementary Figure 3

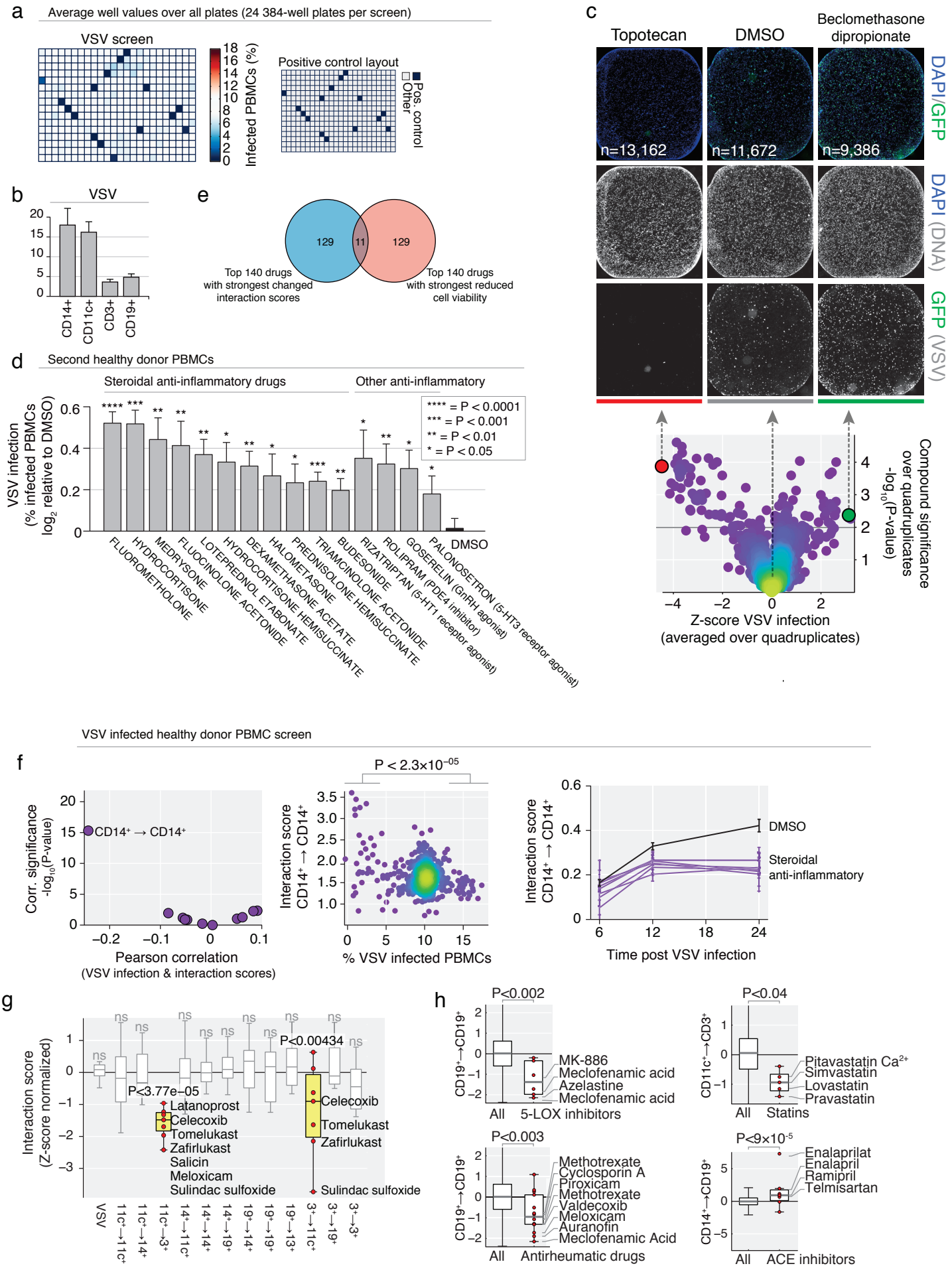

Supplementary Fig. 3. Chemical rewiring of the leukocytic cell-cell contacts, related to Figure 2

(a) Average population-level infection of the VSV screen over all 384-well plates per screen; insert (lower right) indicates positive control layout. (b) Percent infected cells (GFP^+) determined by imaging of each PBMC subset indicated. (c) Example images of merged DAPI and VSV channels (top row), DAPI signal only (middle row) and VSV-GFP signal only (bottom row) after incubation with drugs that decrease infection (Topotecan; left column), show control-level infection (DMSO; middle column) or increase infection (Beclomethasone dipropionate; right column). Merged and representative images cover entire wells of 384-well plates. Shown drugs are highlighted on graph (bottom) indicating VSV infection (x-axis) versus compound effect significance compared to DMSO ($-\log_{10}$(P-value; y-axis). (d) VSV infection in PBMCs of a different healthy donor after incubation with listed compounds, $\log_2$-relative to DMSO infection levels. Mean and standard deviation shown. (e) Venn diagram comparing the top 140 drugs having the largest variation in interaction score (left) to the top 140 with the strongest cytotoxic effect (right), and drugs having both phenotypes (middle). (f) (left panel) Correlation (x-axis) between VSV infection and all measured interaction scores plotted against the correlation significance ($-\log_{10}$(P-value); y-axis); (middle panel) percent VSV infected PBMCs (x-axis) to the $CD14^+ \leftrightarrow CD14^+$ interaction score (y-axis) for each of the 1,402 compounds; (right panel) $CD14^+ \leftrightarrow CD14^+$ interaction scores (y-axis) after incubation with steroidal anti-inflammatory compounds versus DMSO at three time points post virus infection (x-axis). (g-h) Selected interaction scores (y-axis) after treatment with various groups of drugs compared to the corresponding interaction scores over all compounds. (a) Average values over 24 plates are shown. (b) Average and standard deviations over at least 100 DMSO-control wells are shown. (c) Representative images from quadruplicates are shown. (d) Values are averages over at least quadruplicates, with standard deviations over replicates shown. (f) (left) Correlations over all 1,402 compounds, (middle) average values over quadruplicates (x-axis) and duplicates (y-axis) are shown, (right) mean and standard deviation over triplicates per compound are shown. (g-h) Interaction scores are measured at the single cell level, and number of compounds per class are shown in the boxplots.

Supplementary Figure 4

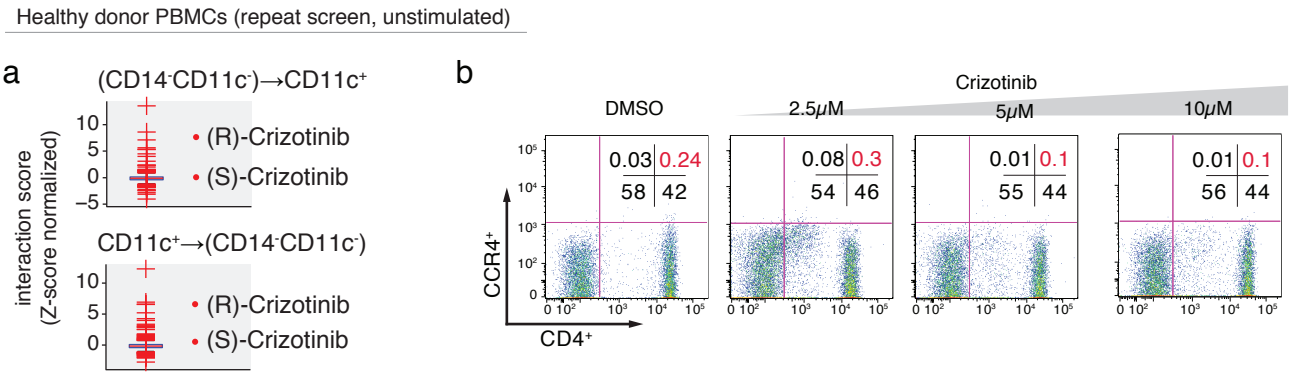

Supplementary Fig. 4. Crizotinib increases interactions between T-cells and antigen presenting cells in naive PBMCs, related to Figure 3

(a) Z-score normalized interaction scores (y-axis) between lymphocytes→$CD11C^+$ and $CD11C^+$→lymphocytes after treatment with (*R*)- and (*S*)-crizotinib are shown, compared to all 1,402 compounds screened (left boxplots). (b) Flow cytometry $CD4^+$, $CCR4^+$ $(CD194)^+$ Th2 T-cells after overnight incubation with (*R*)-crizotinib. (a) Is data from large-scale screens performed in duplicate. (b) is a representative experiment of at least three repeats.

Supplementary Figure 5

SW480 cells

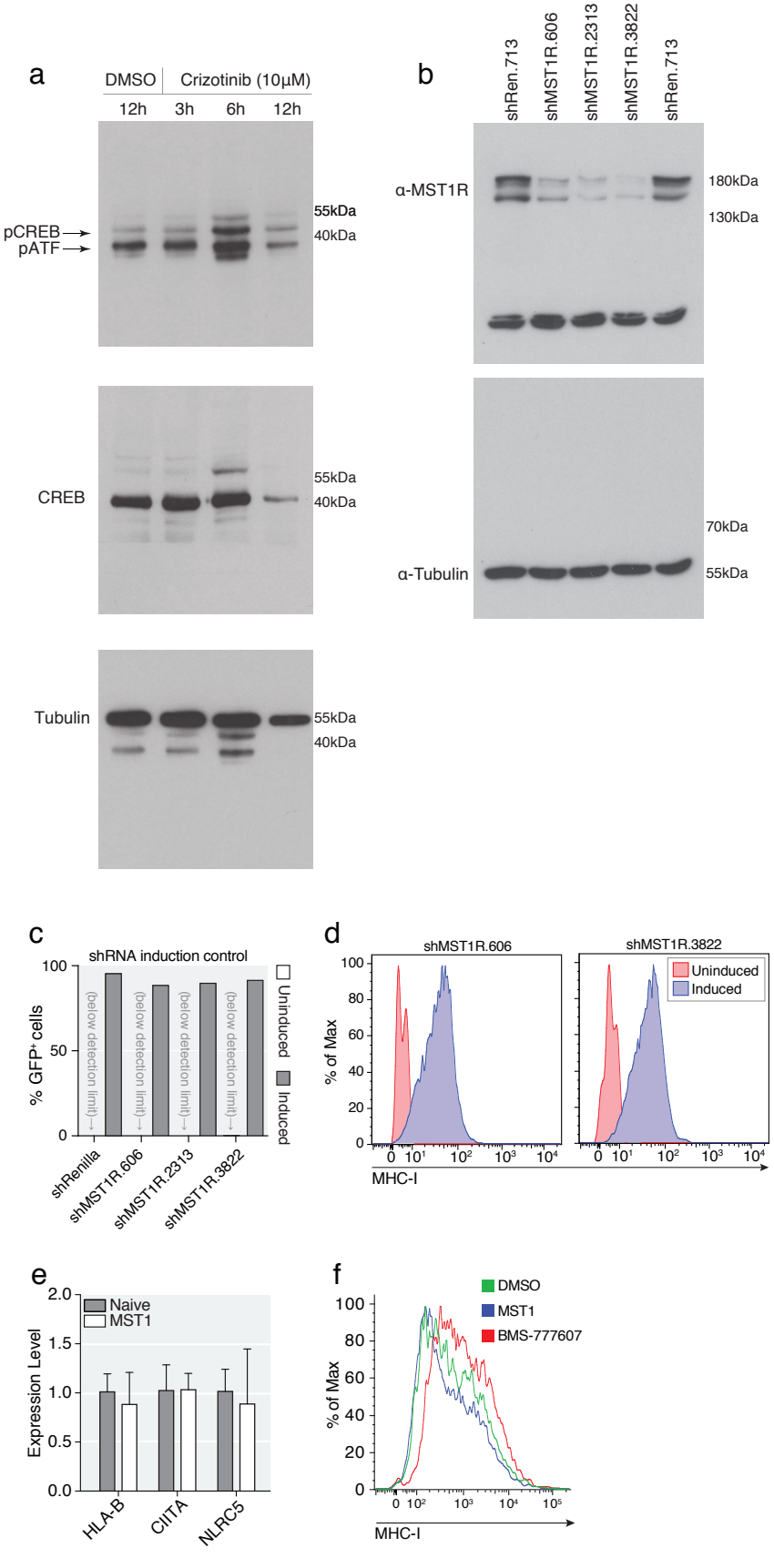

Supplementary Fig. 5. Immunomodulatory effect of crizotinib acts through inhibition of MST1R, related to Figure 5

(a-b) Whole western blots corresponding to Fig. 5d (a) and Fig. 5f (b). (c-d) (c) Percent GFP^+ SW480 cells and (d) MHC-I expression shift after 72h induction of two siRNA against MST1R. (e) qPCR analysis of indicated genes in SW480 cells after incubation with 1μg/ml MST1 or untreated. (f) MHC-I expression after incubation with DMSO (green), 1μM BMS-777607 (red), or 1μg/ml MST1 (blue) overnight on SW480 cells. All experiments are representative examples, performed in at least triplicate, (e) shows standard deviation over technical replicates.

Supplementary Figure 6

Non-small cell lung cancer cell line (H3122), (R)-crizotinib treated (Lovly et al., Nature Medicine, 2014)

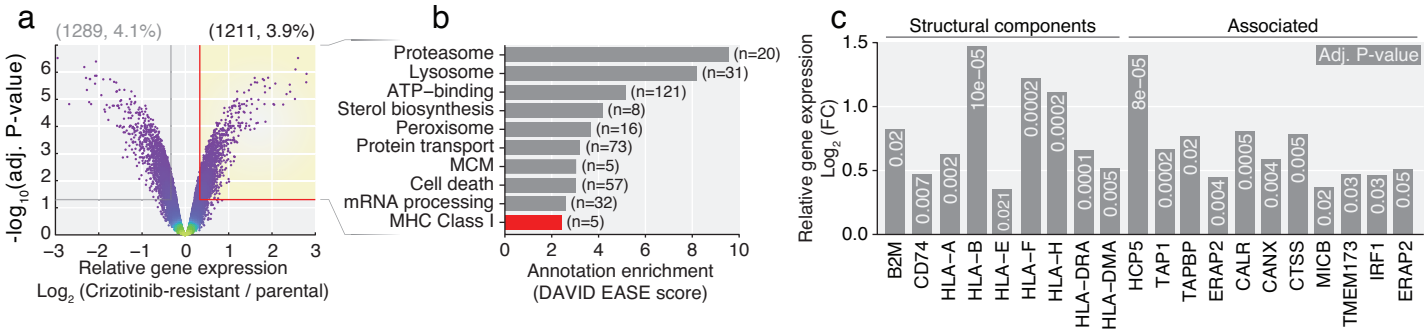

Non-small cell lung cancer cell line (H3122)

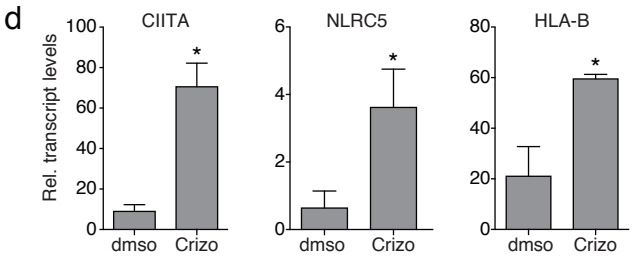

Meta-analysis of MST1R expression in NSCLC (Oncomine 3.0; Rhodes et al., Neoplasia, 2007)

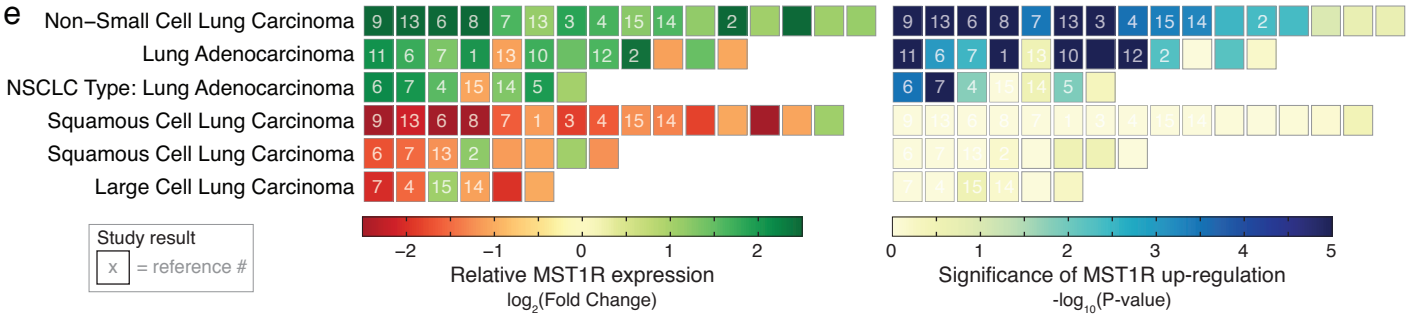

Study references (see also www.oncomine.org):

1. Beer, Nat Med, 2002
2. Bhattacharjee, PNAS, 2001
3. Bild, Nature, 2006
4. Bittner, Not Published, 2005
5. Ding, Nature, 2008
6. Garber, PNAS, 2001
7. Hou, PLoS One, 2010
8. Kuner, Lung Cancer, 2009
9. Lee, Clin Cancer Res, 2008
10. Okayama, Cancer Res, 2012
11. Selamat, Genome Res, 2012
12. Stearman, Am J Pathol, 2005
13. TCGA, No Associated Paper, 2012
14. Tomida, Oncogene, 2004
15. Zhu, J Clin Oncol, 2010

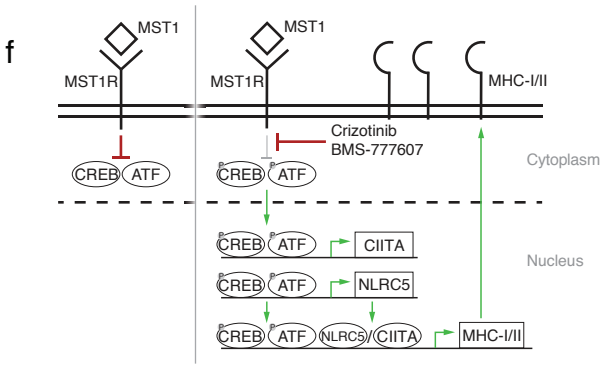

Supplementary Fig 6. *In vivo* assessment of the immunomodulatory properties of crizotinib, related to Figure 6

(a-c) Analysis of publicly available RNAseq of (*R*)-crizotnib treated and untreated H3122 cells [1], mirroring Fig. 4a-c. (d) qPCR of indicated genes after 12h incubation of H3122 cells with DMSO or 10μM crizotinib, normalized to GAPDH. (e) Meta-analysis of relative MST1R expression (left) or significance of MST1R up-regulation (right) in various lung carcinomas. Reference numbers and details are indicated. (f) Schematic of the proposed mechanism by which crizotinib induces MHC-I and –II expression. (a-c) RNAseq performed in triplicate, (d) Is example experiments performed in at least triplicate.

Supplementary Datasets:

Supplementary Dataset 1: Overview of 1,402 compounds used for screens. Each compound is referenced by its SMILES, Chemspider ID, CHEMBL ID, the known drug status, name (from CHEMBL), number of clinical trials involved (clinicaltrials.gov; mid-2015), and the concentration screened, all when available.

Supplementary Dataset 2: Resource: immune modulation potential of 1,402 compounds on key lymphocyte population interaction changes. Each compound is referenced by its common name and SMILES, ranked by their 2-sigma significance to change in virus infection or interaction score. Red: decreasing, or green: increasing, infection or interaction score. Gray boxes indicate not-available due to quality control issues of original images.

Supplementary Dataset 3: RNA sequencing data from SW480 crizotinib treated cells. Analysis is provided in Fig. 4.

Supplementary Tables:

Gene	Ratio	P-value ratio
IRAK1	5.444976626	2.96722E-08
PTK2	5.033641307	2.83287E-05
IRAK3	3.999941922	4.3681E-05
TBK1	3.907688212	2.09359E-05
NUDT1	3.63571038	1.37658E-05
ABL1	3.480377122	9.46978E-08
EPHA2	3.469463575	3.79272E-05
MST1R	3.418151364	1.08821E-05
SLK	3.351418171	1.46759E-07
ABL2	2.991396279	0.001733557
AZI2	2.796944999	5.80454E-06
EML4	2.737025387	0.000685321
ACVR1	2.698848643	1.27077E-05
PTK2B	2.551794377	0.001600094
ALK	2.31509025	0.00857899
KRT78	0.360217134	1.02565E-05

Supplementary Table 1: Chemical proteomics of crizotinib in H3122 cells. iTRAQ ratios and p-values are provided to assess quantitative interactions, as in [2-3].

Supplementary Table 2. Small molecule screening data

Category	Parameter	Description
Assay	Type of assay	*Ex vivo*, whole primary human materia (PBMC)l, peripheral blood.
	Target	Spatial orientation / cell-cell contacts of cells.
	Primary measurement	Image based screening of PBMC subpopulations as indicated by fluorescent antibodies against specific surface markers; and the physical distance of these cells to each other.
	Key reagents	Anti-human CD19 (HIB19, APC), CD11c (3.9, APC), CD3 (HIT3a, PE), CD14 (61D3, PE), and CD34 (4H11, APC) from eBiosciences, CD20 (2H7, GFP) from BD Biosciences, and CD56 (A07788, PE) from Beckman Coulter, DAPI (Sigma)
	Assay protocol	The method is described in Vladimer et al, Nature Chemical Biology, 2017. Online Methods
	Additional comments	
Library	Library size	1402 entities
	Library composition	50% FDA approved drugs, 50% tool compounds or other small molecules
	Source	See methods, Vladimer et al, Nature Chemical Biology, 2017, online methods; and gifts from various sources
	Additional comments	
Screen	Format	384-well plates
	Concentration(s) tested	10uM concentration
	Plate controls	DMSO (negative control), 10uM digitoxin (positive control) (52 wells total, scattered throughout plate). Randomized duplicate or quadruplicate of compounds.
	Reagent/ compound dispensing system	Compounds: ECHO transfer system, reagents: Janus with a 96- and 384-head (Perkin Elmer)
	Detection instrument and software	Please see PLACBO platform, CeMM. Supplemented with a Perkin Elmer Opera Phenix
	Assay validation/QC	Randomized layout for plate effects, average and s.d. of single-cell phenotypes.
	Correction factors	Image illumination correction, background correction, plate-effect correction,
	Normalization	Positive and negative controls
	Additional comments	
Post-HTS analysis	Hit criteria	Interactions of cells were scored positive if the nuclear centers were within 10 pixels, and all interactions measured per well. Hits were drugs which increased or decreased these measurements by 2 sigma.
	Hit rate	11%; but not a random library, see Vladimer et al. Nature Chemical Biology, 2017
	Additional assay(s)	Key compounds were followed-up with other biochemical means. See Vladimer et al, Nature Chemical Biology, 2017.
	Confirmation of hit purity and structure	Compounds were purchased from reputable vendors, or gifts from known sources. Random compounds were QC'd prior to screen by mass spectrometry.
	Additional comments	

Supplementary Table 2: Small molecule screening data table.

Supplementary References:

1. Lovly, C.M. et al. Rationale for co-targeting IGF-1R and ALK in ALK fusion-positive lung cancer. *Nat Med* **20**, 1027-34 (2014).
2. Winter, G.E. et al. Systems-pharmacology dissection of a drug synergy in imatinib-resistant CML. *Nature chemical biology* **8**, 905-912 (2012).
3 Huber, K.V.M. et al. Stereospecific targeting of MTH1 by (S)-crizotinib as an anticancer strategy. *Nature* **508**, 222-227 (2014).